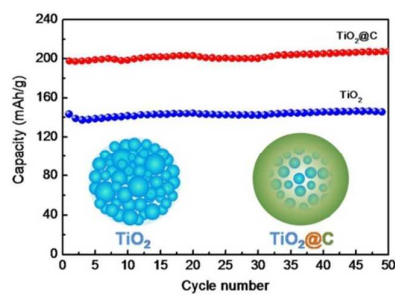


**TiO<sub>2</sub>@C Composite Nanospheres with an Optimized Homogeneous Structure for Lithium-ion Batteries**

Journal:	<i>New Journal of Chemistry</i>
Manuscript ID:	NJ-ART-02-2014-000263.R2
Article Type:	Paper
Date Submitted by the Author:	16-May-2014
Complete List of Authors:	Zhang, Jun; University of Jinan, Ni, Jiangfeng; Soochow University, Guo, Jing; University of Jinan, Cao, Bingqiang; University of Jinan,

## Table of contents entry



TiO<sub>2</sub>@C nanospheres synthesized by pyrolysis demonstrate enhanced performance as an anode for lithium-ion batteries.

## ARTICLE

# TiO<sub>2</sub>@C Composite Nanospheres with an Optimized Homogeneous Structure for Lithium-ion Batteries

Cite this: DOI: 10.1039/x0xx00000x

Jun Zhang,<sup>\*a,c</sup> Jiangfeng Ni,<sup>b</sup> Jing Guo<sup>a</sup> and Bingqiang Cao<sup>\*a</sup>,

Received 00th January 2012,

Accepted 00th January 2012

DOI: 10.1039/x0xx00000x

www.rsc.org/

Homogeneous TiO<sub>2</sub>@C composite nanospheres are synthesized by a direct pyrolysis strategy using Ti-containing organic-inorganic polymers as the precursor. The TiO<sub>2</sub>@C composite nanospheres possess uniform distribution of tiny TiO<sub>2</sub> nanoparticles confined in carbon matrix with a homogeneous structure. The carbon phase can not only improve the conductivity but also prevents the aggregation of TiO<sub>2</sub> nanoparticles. When evaluated as an anode for lithium-ion batteries, the TiO<sub>2</sub>@C nanocomposites demonstrate high reversible specific capacity of 207 mAh g<sup>-1</sup> at 0.5C (1C = 250 mA g<sup>-1</sup>) after 50 cycles and stable cycling performance in comparison to pure TiO<sub>2</sub> nanospheres. This work offers a new pathway for realization of carbon-based composite materials for use as high performance anodes in LIBs.

## Introduction

Lithium-ion batteries (LIBs) have been considered as one of the most promising energy storage and conversion technology to fulfil the ever-growing demand in both small consumer electronic devices and large-scale applications, such as electric vehicles (EV), hybrid electric vehicles (HEV), and stationary energy storage<sup>1,2</sup>. Practical applications of LIBs critically relied on the electrode materials with high capacity, high rate capability, good stability and safety. The current widely used anode in LIBs is graphite. In spite of its excellent electrical conductivity, graphite anode suffers from low Li-ion diffusion coefficient and risk of lithium dendrites formation, which might cause serious safety problems<sup>3</sup>.

TiO<sub>2</sub>, as one of the most investigated semiconductor metal oxides, has attracted considerable attention for application in many fields, such as solar cells, photocatalysis, gas sensors, and LIBs<sup>4-8</sup>. For use as an anode for LIBs, TiO<sub>2</sub> features by a series of merits including the low cost, low toxicity, high capacity, high current rate performance, and improved electrochemical stability<sup>3</sup>. However, the poor electronic and Li-ion conductivity have significantly limited its potential application in LIBs. To alleviate such problems, many strategies have been developed to improve the performances of TiO<sub>2</sub> anodes. For example, the controllable fabrication of TiO<sub>2</sub>-based nanomaterials with desired structures or morphologies has proved to be very effective to improve the LIBs performances. Lou et al.<sup>9,10</sup> have demonstrated that TiO<sub>2</sub> hollow nanostructures could deliver better properties in terms of higher capacity, better rate capability, and good cycling performance. TiO<sub>2</sub> nanosheets with engineered (001) crystal facets have manifested enhanced electrochemical performances due to the accelerated Li-ion diffusion kinetics in specific crystal direction and adequate

electrode–electrolyte contact<sup>11,12</sup>. Decreasing the particle size from micrometer to the nanometer scale is also a key to improved Li-ion diffusion because of the reduced diffusion length<sup>2,13</sup>. Ren et al. have shown that TiO<sub>2</sub> nanoparticles with the ever smallest size (< 4.3 nm) are superior in Li-ion and charge storage compared with other bulk, nanowires, and nanotubes morphologies<sup>14</sup>.

While great progress has been obtained by the nanostructuring strategy, a well-established and more reliable approach is to fabricate composite electrode materials by coating or mixing a host material with guest additives such as conductive carbon<sup>15-18</sup>. Great improvement in the specific capacity, rate performance, and cycling stability can be expected, because the carbon additive could significantly improve the surface electronic conductivity and the electric contact between electrodes and surrounding active agents<sup>15</sup>. Zhao et al. have proposed to incorporate a 3D carbon mixed conducting network in electrode materials, which allows for both fast Li-ion and electron migration<sup>19</sup>. TiO<sub>2</sub>@carbon composite nanofibers prepared by combination of electrospinning and subsequent thermal treatments also exhibited excellent cycling stability and rate capability as an anode material<sup>20</sup>. Park et al.<sup>21,22</sup> have reported carbon-coated TiO<sub>2</sub> nanotubes with very low carbon content synthesized could manifest high rate capability and power performance. Wang<sup>23</sup> and Guo<sup>24</sup> et al. have reported mesoporous TiO<sub>2</sub>/C composite anodes with excellent rate capability and cycling performance. Very recently, Petkovich<sup>25</sup> and Wang<sup>26</sup> et al. used one-pot pyrolysis to produce 3DOM TiO<sub>2</sub>/C and CNT@TiO<sub>2</sub>-C composite materials for LIBs anodes with high rate performance. To further optimize the electrochemical performance of TiO<sub>2</sub>-based anodes with low cost, it is desirable

to develop a simple procedure for synthesizing  $\text{TiO}_2$ @carbon composite anode materials, in which nanometer-sized  $\text{TiO}_2$  particles are homogeneously dispersed in conductive carbon matrix. Such an optimized structure would enable fast electron transport between nanoparticles, thus improving the electrochemical performance.

In this work, we propose a direct pyrolysis route at moderate temperature to prepare homogeneous  $\text{TiO}_2$ @C composite nanospheres by using Ti-containing colloidal organic-inorganic polymers as the precursor. The new attempt using organic-inorganic polymer spheres as both carbon and  $\text{TiO}_2$  sources has advantages of generation of carbon phase closely coated on  $\text{TiO}_2$  nanoparticles and suppression of the particle growth to yield homogeneous conductive nanocomposite. When evaluated as the anodes for LIBs, the  $\text{TiO}_2$ @C composite nanospheres manifest excellent charge-discharge properties with relatively high capacity, good rate capability, and stable cycling performance.

## Experimental Section

### Synthesis of homogeneous $\text{TiO}_2$ @C composite nanospheres

Organic-inorganic polymer nanospheres containing Ti were prepared according to the literature method with some modifications<sup>27,28</sup>. In a typical synthesis, 2 mL tetrabutyl titanate (TBT) was added to 50 mL ethylene glycol (EG) under magnetic stirring for 10 h, then the mixture was transferred into a solution containing 2.7 mL water and 170 mL acetone. After further stirring for 1 h, the white colloidal organic-inorganic polymers were harvested by centrifugation and washing with water and ethanol several times, and dried at 80 °C. The as-obtained organic-inorganic nanospheres are indeed titania glycolate polymers and have an amorphous structure<sup>27</sup>. Homogeneous  $\text{TiO}_2$ @C nanocomposites were readily obtained by pyrolysis of the organic-inorganic nanospheres in  $\text{N}_2$  atmosphere at 500 °C for 4 h. For comparison, pristine  $\text{TiO}_2$  nanospheres were also synthesized by annealing the polymers in air at 500 °C for 4 h.

### Characterization

The crystal phase and structure of samples were identified by power X-ray diffraction (XRD) using a Bruker diffractometer (D8-Advance) with  $\text{Cu K}\alpha$  radiation of 1.5418 Å. Thermal-gravimetric analysis (TG) was performed on Mettler-Toledo TGA/DSC 1/1600HT at a heating rate of 5 °C/min in air. The size, morphology and composition of the samples were characterized by scanning electron microscope (SEM, Quanta FEG 250, 30 kV) and transmission electron microscope (TEM, JEM-1011, 100 kV), high resolution transmission electron microscope (HRTEM, JEOL-2010, 200kV), energy dispersive X-ray spectroscopy (EDS, JEOL-2010, 200kV), and  $\text{N}_2$  adsorption-desorption (JW-BK122W).

### Electrochemical characterization

2032 coin-type cells were used for electrochemical test. The composite electrode sheets consisting of 70 wt.% active material, 20 wt.% acetylene black, and 10 wt.% polytetrafluoroethylene (PTFE) was used as cathode. Lithium metal foil was used as counter and reference electrodes. The electrolyte solution is 1M LiPF<sub>6</sub> dissolved in a mixture of ethylene carbonate (EC) and dimethyl carbonate (DMC) with a volume ratio of 1:1. Galvanostatic tests were carried out using a Land battery test system at 28 °C (1 C was defined as 250 mA g<sup>-1</sup>). Electrochemical impedance spectroscopy (EIS) tests were performed on a Zennium electrochemical workstation tester.

## Results and discussion

### Morphology and structure investigation

The Ti-containing organic-inorganic polymer nanospheres were prepared by an improved sol-gel method, by which the hydrolysis of TBT was controlled to occur slowly to obtain a homogeneous nucleation and growth<sup>27</sup>. Fig. 1a shows that the polymer nanospheres have a sphere-like shape, and some spheres are seen to fuse together. The inset of Fig. 1a is the size distribution histogram, which indicates the nanospheres have a diameter in the range of 250-550 nm, with an average size of 377 nm. After calcination at a moderate temperature of 500 °C in  $\text{N}_2$ , the organic-inorganic polymers can be converted into  $\text{TiO}_2$ @C nanospheres. Fig. 1b displays the SEM image of the composite  $\text{TiO}_2$ @C nanospheres, revealing that the  $\text{TiO}_2$ @C nanospheres well preserve the spherical morphology after thermal annealing. Interestingly, the  $\text{TiO}_2$ @C nanospheres have a smaller size as compared with the polymer precursor of Fig. 1a. The reduced size and dimension of the composite nanospheres is probably caused by remove of water and decomposition of organic component under the annealing process, resulting in the shrinkage of precursor spheres.

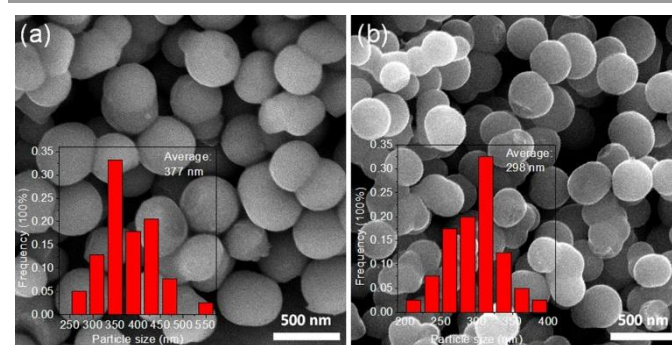
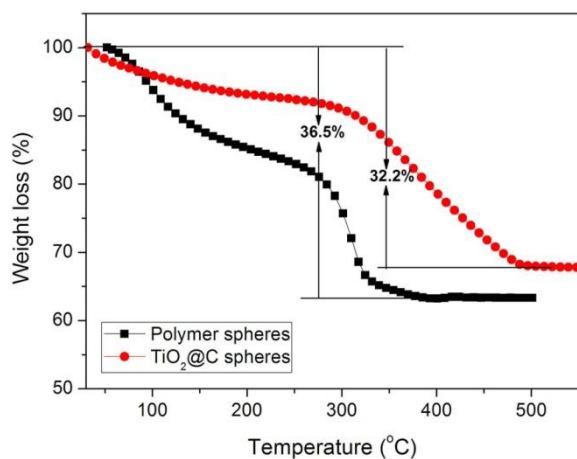


Fig. 1. SEM images of (a) Ti-containing organic-inorganic polymers and (b)  $\text{TiO}_2$ @C composite nanospheres obtained by pyrolysis of the Ti-containing polymers.

The thermal behavior of the precursor polymer and  $\text{TiO}_2$ @C spheres has been examined by TG analysis. In Fig. 2, the TG curve of precursor polymer reveals a total weight loss of 36.5%, consisting of two steps of weight loss that can be ascribed to the evaporation of water molecules before 150 °C and the thermal decomposition or combustion of organic compounds such as

ethylene glycol in the polymers between 150 and 400 °C. The curve for TiO<sub>2</sub>@C spheres also contains two steps of weight loss of water evaporation and combustion of the thermally decomposed carbon phase. The carbon content in the TiO<sub>2</sub>@C spheres is about 32.2 %.



**Fig. 2.** TG analysis of Ti-containing organic-inorganic polymer and TiO<sub>2</sub>@C nanospheres.

The crystalline phase of the polymer precursor and TiO<sub>2</sub>@C nanospheres has been studied by XRD. Fig. 3 demonstrates that the polymer precursor has an amorphous structure, while the TiO<sub>2</sub>@C sample shows a dominant structure of rutile TiO<sub>2</sub> (JCPDS No.65-0190) and a trace amount of anatase TiO<sub>2</sub> (JCPDS No. 21-1272) indicated by an asterisk. The crystallite size of TiO<sub>2</sub>@C is estimated to be 11.2 nm from the full width at half maximum (FWHM) of (211) diffraction peak by using Scherer equation. After annealing under N<sub>2</sub> atmosphere, the organic compounds in the precursor would be carbonized through pyrolysis and eventually transform into carbon.

Detailed structure and morphology of the samples have been further characterized by TEM. Fig. 4(a-d) exhibits the

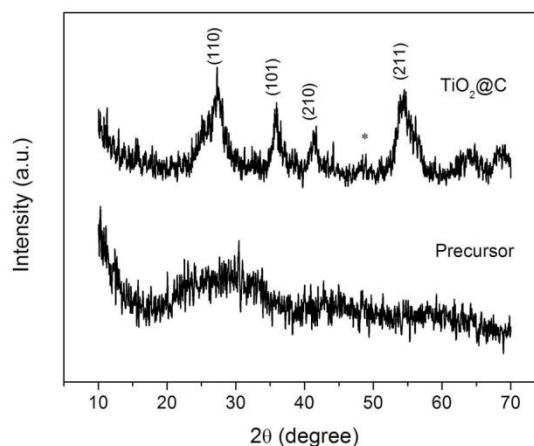


**Fig. 3.** XRD patterns of the polymer precursor and TiO<sub>2</sub>@C nanospheres.

representative TEM images of TiO<sub>2</sub>@C nanospheres with different magnifications. As can be seen in Fig. 4a and b, the TiO<sub>2</sub>@C particles have a sphere-like morphology. Closer observation from the individual nanosphere in Fig. 4b reveals that the TiO<sub>2</sub>@C nanosphere shows a homogenous structure. From Fig. 4c, it is seen that the sphere contains many discrete nanoparticles confined in carbon matrix with a small size of 8-18 nm. Under annealing in N<sub>2</sub>, the organic molecules cannot burn off and subsequently convert into carbon through pyrolysis. During the carbonization process at 500 °C in N<sub>2</sub>, TiO<sub>2</sub> nanoparticles are formed with better crystallization and simultaneously carbon phase is formed around the TiO<sub>2</sub> nanoparticles, leading to the formation of a homogeneous nanocomposite of TiO<sub>2</sub>@C with TiO<sub>2</sub> nanoparticles highly distributed in carbon. The inset of Fig. 4c illustrates the homogeneous structure of the TiO<sub>2</sub>@C composite nanospheres. Fig. 4d shows the HRTEM image of a TiO<sub>2</sub>@C nanosphere. A carbon layer around the sphere edge can be seen clearly, as indicated by the arrows. The clear lattice fringes reveal the high

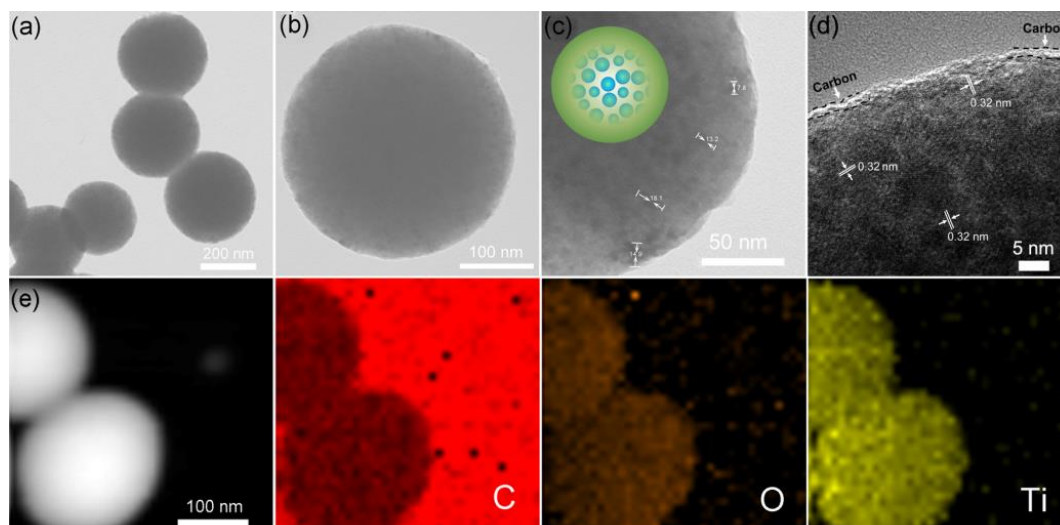


**Fig. 4.** (a-c) TEM, (d) HRTEM images and (e) Element mapping of TiO<sub>2</sub>@C nanospheres.

## ARTICLE

crystalline nature of the  $\text{TiO}_2$  nanoparticles confined in carbon. The interplane spacing of 0.32 nm corresponds to the (110) planes of rutile  $\text{TiO}_2$ . The elemental composition of the sample was further studied by the local EDS element mapping

technique mounted to HRTEM. The results are shown in Fig. 4e. It is apparent that the particle has uniform distributions of all the elements (C, O, and Ti), further demonstrate the homogeneous structure of  $\text{TiO}_2@\text{C}$  composite nanospheres.

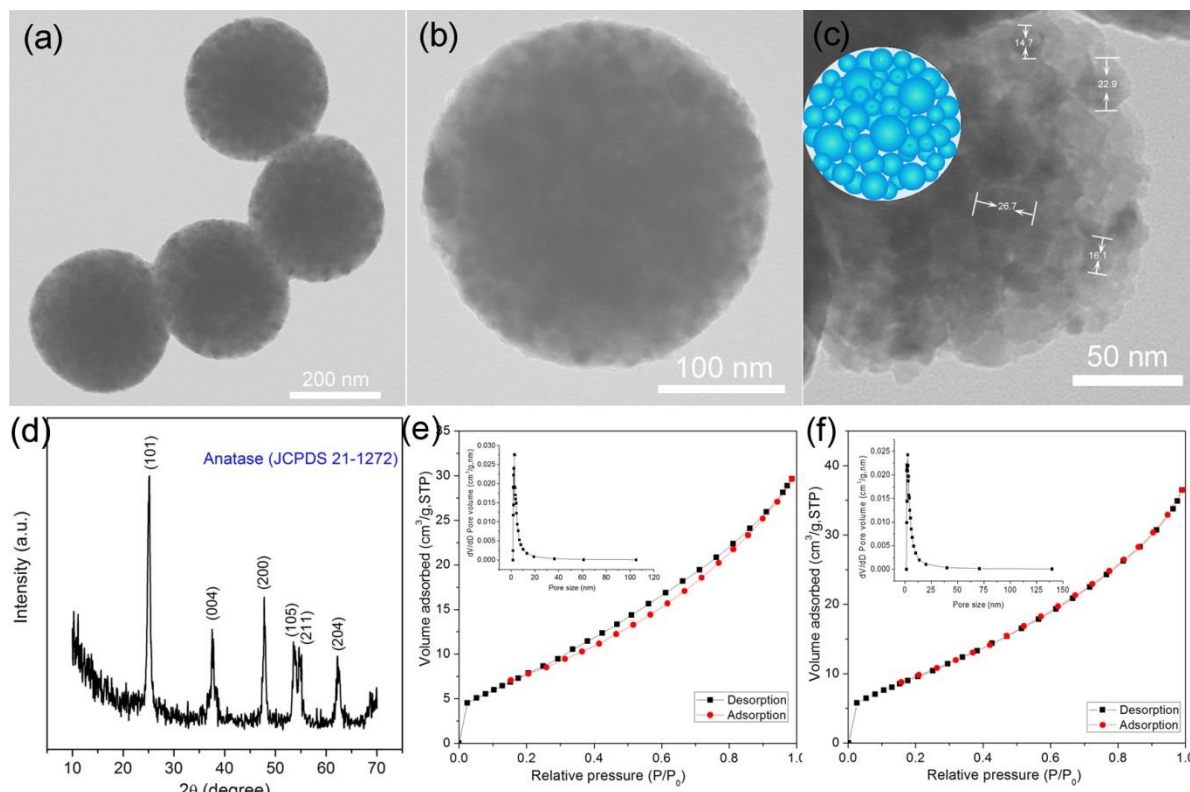


**Fig. 5.** (a-c) TEM images and (d) XRD pattern of pure  $\text{TiO}_2$  nanospheres obtained by calcination of the Ti-containing polymers in air, and  $\text{N}_2$  adsorption-desorption analysis of (e)  $\text{TiO}_2$  and (f)  $\text{TiO}_2@\text{C}$ .

For comparison, pure  $\text{TiO}_2$  nanospheres were also prepared by directly anneal the Ti-containing organic-inorganic polymer nanospheres in air. Fig. 5(a-c) exhibits the SEM images of pure  $\text{TiO}_2$  nanospheres. As can be seen in Fig. 5a and b, the  $\text{TiO}_2$  particles also possess a sphere-like morphology. By closer observation from the individual nanospheres in Fig. 5b and 4b, it reveals that the former has a relatively rough surface. Nanoparticles with different diameters can be easily distinguished out due to the image contrast. Fig. 5c indicates the  $\text{TiO}_2$  nanosphere is comprised of numerous aggregated nanoparticles with a size range of 14-27 nm. When calcined in air, the organic component in the polymer spheres could be completely removed and  $\text{TiO}_2$  nanoparticles nucleated and grew together to constitute the spheres. The inset schematic illustration of Fig. 5c simulates the structure of pure  $\text{TiO}_2$

nanospheres, which is assembled by many  $\text{TiO}_2$  nanoparticles with different size. The XRD pattern in Fig. 5d suggests the pure  $\text{TiO}_2$  nanospheres have an anatase structure, with all the diffraction peaks being consistent with JCPDS 21-1272. The mean crystallite size estimated from the full width at half maximum (FWHM) of the (101) peak is ca. 17.7 nm, which is much larger than that (11.2 nm) of  $\text{TiO}_2@\text{C}$  composites. This indicates that the annealing atmosphere has a significant influence on the crystallite size of the products. Annealing in air is able to burn off the organic component and obtain pure inorganic  $\text{TiO}_2$  nanospheres. If the annealing process is performed in  $\text{N}_2$ , the organic compounds will be carbonized through pyrolysis and eventually transform into carbon. It is deduced that the formed carbon around the  $\text{TiO}_2$  could effectively suppress the growth of  $\text{TiO}_2$  nanoparticles. Recent

works by Petkovich<sup>25</sup> and Huang et al.<sup>29</sup> reported the similar result at temperature of 800 and 1100 °C. The Brunauer–Emmett–Teller (BET) specific surface area and porous structure of TiO<sub>2</sub> and TiO<sub>2</sub>@C have been obtained by N<sub>2</sub> adsorption-desorption, which is shown in Fig. 5e and f. The BET surface area of TiO<sub>2</sub> is evaluated to be 36.8 m<sup>2</sup>/g, which is a little larger than that (31.1 m<sup>2</sup>/g) of TiO<sub>2</sub>@C composite. This is because the pure TiO<sub>2</sub> nanospheres are an aggregation of TiO<sub>2</sub> nanoparticles with rich inner-particle space. Furthermore, the insets in Fig. 5e and f are the Barrett–Joyner–Halenda (BJH) pore size distribution, revealing

both samples have a mesoporous structure with pore size in the range of 2–50 nm.

### Electrochemical performance

Such a TiO<sub>2</sub>@C structure is very promising for use as LIBs anode materials, as the carbon component can greatly enhance the electronic conductivity between the TiO<sub>2</sub> nanoparticles. In addition, the carbon matrix can also effectively prevent the aggregation of nanoparticles during cycling<sup>30</sup>.

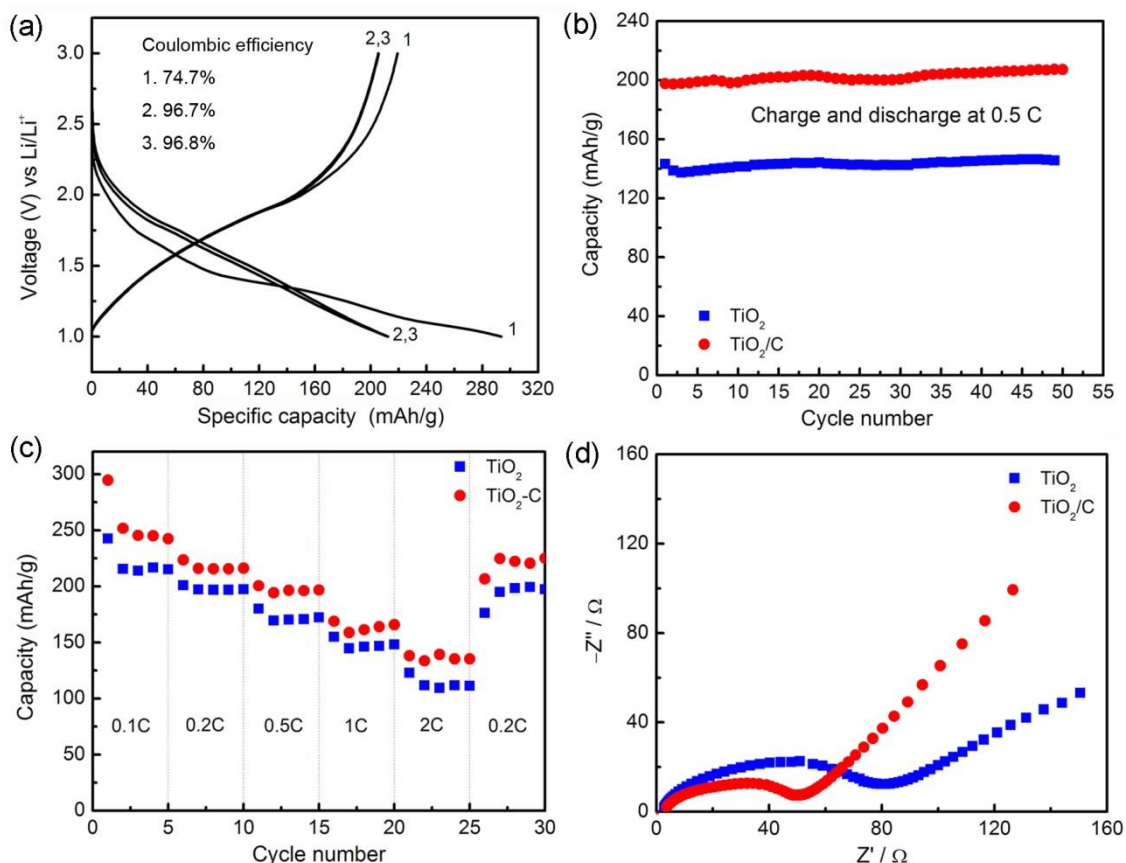


**Fig. 6.** (a) Discharge/charge voltage profiles at 0.2C, (b) cycling performance at 0.5C, (c) rate capability from 0.1C to 2C, and (d) Nyquist plots of TiO<sub>2</sub> and TiO<sub>2</sub>@C nanospheres.

We thus further evaluate the electrochemical performances of these unique homogeneous TiO<sub>2</sub>@C nanospheres for LIBs. Fig. 6a shows the first three consecutive discharge/charge voltage profiles of the TiO<sub>2</sub>@C composite nanospheres at a 0.2C rate in the voltage range of 1.0–3.0 V. The initial discharge and charge capacities are found to be 293.6 and 219.3 mAh g<sup>-1</sup>, indicating an initial coulombic efficiency of 74.7%. Such an initial discharge capacity is even higher than the theoretical capacity (233 mAh g<sup>-1</sup>) of TiO<sub>2</sub>@C nanospheres. The theoretical capacity of TiO<sub>2</sub>@C nanospheres is calculated based on the weight content and theoretical capacity of TiO<sub>2</sub> (67.8 wt%, 168 mAh g<sup>-1</sup>) and carbon (32.2 wt%, 372 mAh g<sup>-1</sup>). The extra lithium storage capacity might be associated with the phenomenon of interface storage due to the unique composite

structure and the carbon phase. While for the second and third cycle, the discharge and charge capacities are 212.2 and 205.4 mAh g<sup>-1</sup> and 212.3 and 205.7 mAh g<sup>-1</sup>, corresponding to a coulombic efficiency of 96.7% and 96.8%. Compared with the initial discharge capacity (293 mAh g<sup>-1</sup>), the second discharge shows an irreversible capacity of 80 mAh g<sup>-1</sup>. The capacity loss may be caused by the inserted Li-ions in the irreversible sites of TiO<sub>2</sub> nanoparticles<sup>31,32</sup> and other side reactions arising from trace water absorbed on electrode materials<sup>32</sup> at the first stage of discharge-charge process. Similar phenomenon has also been previously observed for various TiO<sub>2</sub> polymorphs, such as TiO<sub>2</sub>(B)<sup>12,33</sup>, anatase<sup>19,20</sup>, and rutile<sup>31,34</sup>.

The cycling performance of pure TiO<sub>2</sub> and TiO<sub>2</sub>@C composite nanospheres has been tested at 0.5C. As shown in

Fig. 6b, although both  $\text{TiO}_2@\text{C}$  and  $\text{TiO}_2$  exhibit good cycling stability, the  $\text{TiO}_2@\text{C}$  nanocomposite possesses apparently much higher capacity than pure  $\text{TiO}_2$ . The higher capacity of  $\text{TiO}_2@\text{C}$  might be due to the carbon phase, which has a higher theoretical capacity than  $\text{TiO}_2$ . After 50 cycles of discharge/charge at 0.5C, the  $\text{TiO}_2@\text{C}$  nanospheres can still deliver a high reversible specific capacity of  $207 \text{ mAh g}^{-1}$ , which is much higher than that ( $145.6 \text{ mAh g}^{-1}$ ) of pure  $\text{TiO}_2$  nanospheres and is also better than the reported results for  $\text{TiO}_2/\text{C}$  nanocomposite<sup>20,24,35,36</sup> and  $\text{TiO}_2$  nanotubes<sup>8</sup> and nanoparticles<sup>37</sup> at a similar current density. In addition, the pure  $\text{TiO}_2$  nanospheres have an anatase structure, which is generally considered to be more electrochemically active than the rutile polymorph for Li-insertion<sup>38,39</sup>. The above results clearly demonstrate the superior lithium storage performance of rutile  $\text{TiO}_2$ -based composite to anatase as an anode material.

The rate capability of the  $\text{TiO}_2@\text{C}$  nanospheres is also tested at different current densities. As shown in Fig. 6c, the  $\text{TiO}_2@\text{C}$  anode is observed to exhibit much higher reversible capacity and good cycling stability than  $\text{TiO}_2$ . The  $\text{TiO}_2@\text{C}$  nanocomposite presents very good cycling response to continuously varying current rates from 0.1 to 2C. At various current densities, the  $\text{TiO}_2@\text{C}$  composite anode can retain discharge capacities of 242.6, 216.2, 197.1, 165.5 and  $134.3 \text{ mAh g}^{-1}$  after 5 cycles at each current rates of 0.1, 0.2, 0.5, 1 and 2C, respectively, while the pure  $\text{TiO}_2$  nanospheres only deliver discharge capacities of 215.5, 196.7, 172.1, 147.3 and  $110.6 \text{ mAh g}^{-1}$ . Furthermore, when the discharge-charge test is re-cycled at 0.2C after 2C, the  $\text{TiO}_2@\text{C}$  nanocomposite can still deliver a discharge capacity of about  $220 \text{ mAh g}^{-1}$ . This value is almost identical to the former 0.2C test, suggesting a high electrochemical stability of the homogenous  $\text{TiO}_2@\text{C}$  nanocomposites.

In order to understand the improved performance of  $\text{TiO}_2@\text{C}$  nanocomposites, the electrochemical impedance spectra (EIS) tests for both  $\text{TiO}_2@\text{C}$  and pure  $\text{TiO}_2$  have been performed. As displayed in Fig. 6d, the Nyquist plots of both  $\text{TiO}_2@\text{C}$  and pure  $\text{TiO}_2$  consist of one semicircle in the high-frequency region and a bias line in the low-frequency region. The radius of the semicircle is correlated with the charge-transfer ability of the corresponding electrode. Apparently, the  $\text{TiO}_2@\text{C}$  electrode possesses a much lower resistance ( $50 \Omega$ ) than the pure  $\text{TiO}_2$  electrode ( $81 \Omega$ ), as a result of the good electrical contact between  $\text{TiO}_2$  and carbon. This indicates that the  $\text{TiO}_2@\text{C}$  composite electrode possesses lower charge-transfer impedance due to the uniform carbon matrix around  $\text{TiO}_2$  nanoparticles. Consequently, both the  $\text{Li}^+$  diffusion and electron transfer are effectively expedited at high cycling rates for the  $\text{TiO}_2@\text{C}$  composite electrode, leading to superior capacity retentions at different current rates in comparison to pure  $\text{TiO}_2$  nanospheres.

Based on the above discussion, the  $\text{TiO}_2@\text{C}$  nanocomposite has demonstrated much better performance than the pure  $\text{TiO}_2$  anode. Several factors may account for the enhanced lithium storage properties. First, the  $\text{TiO}_2@\text{C}$  has higher electronic conductivity for electron transfer due to the uniform carbon coating<sup>20,24,30,35,40</sup>. Second, the small size of  $\text{TiO}_2$  nanoparticles

confined in carbon also provides a short path for lithium intercalation and de-intercalation<sup>14,31</sup>. Third, the optimized homogeneous  $\text{TiO}_2@\text{C}$  structure might also contribute to the improved performance, as it delivers a higher capacity during cycling when compared with other forms of  $\text{TiO}_2/\text{C}$  nanocomposite<sup>24,35,36</sup>, possibly because the carbon matrix could effectively prevent the aggregation of  $\text{TiO}_2$  nanoparticles.

## Conclusions

In summary, a direct pyrolysis strategy has been proposed to realize an optimized structure of homogenous  $\text{TiO}_2@\text{C}$  nanocomposite by using Ti-containing organic-inorganic polymers as the precursor. The organic component can be easily converted to carbon, which can effectively suppress the growth of nucleated  $\text{TiO}_2$  nanoparticles and simultaneously make the  $\text{TiO}_2$  nanoparticles highly distributed in the carbon matrix. Electrochemical tests demonstrate the as-synthesized  $\text{TiO}_2@\text{C}$  composite nanospheres exhibit improved Li-ion storage performance in terms of higher capacity, better cycling performance and rate capability compared with pure  $\text{TiO}_2$  nanospheres. The enhanced properties can be ascribed to the unique homogeneous structure of  $\text{TiO}_2@\text{C}$ , small size of  $\text{TiO}_2$  nanoparticles, and improved conductivity due to the carbon matrix. It is expected that the proposed direct pyrolysis route in this work can also be utilized to fabricate other composite electrode materials for high performance lithium-ion batteries.

## Acknowledgements

This work is supported by the Program for New Century Excellent Talents in University (NCET-11-1027) of MOE, China, the Taishan Scholar Professorship (TSHW20091007), the Open Project of Key Laboratory of Advanced Energy Materials Chemistry of Nankai University (KLAEMC-OP201201), and Shandong Provincial Science Foundation for Disguised Youth Scholars (JQ201214) and Excellent Young and Middle-aged Scientists (BS2012CL003).

## Notes and references

- a Key Laboratory of Inorganic Functional Materials in Universities of Shandong, School of Materials Science and Engineering, University of Jinan, Jinan 250022, China.  
E-mail: mse\_zhangj@ujn.edu.cn; mse\_caobq@ujn.edu.cn
- School of Energy, Soochow University, Suzhou 215006, China.
- Key Laboratory of Advanced Energy Materials Chemistry (Ministry of Education), Collaborative Innovation Center of Chemical Science and Engineering (Tianjin), College of Chemistry, Nankai University, Tianjin 300071, China.
1. B. Dunn, H. Kamath and J.-M. Tarascon, *Science*, 2011, **334**, 928–935.
2. P. G. Bruce, B. Scrosati and J. M. Tarascon, *Angew. Chem. Int. Ed.*, 2008, **47**, 2930–2946.
3. G.-N. Zhu, Y.-G. Wang and Y.-Y. Xia, *Energy & Environmental Science*, 2012, **5**, 6652–6667.
4. J. Qu, Q. D. Wu, Y. R. Ren, Z. Su, C. Lai and J. N. Ding, *Chemistry—An Asian Journal*, 2012, **7**, 2516–2518.
5. X. Chen and S. S. Mao, *Chem. Rev.*, 2007, **107**, 2891–2959



6. J. F. Qian, M. Zhou, Y. L. Cao, X. P. Ai and H. X. Yang, *J. Phys. Chem. C*, 2010, **114**, 3477-3482.
7. A. S. Aricò, P. Bruce, B. Scrosati, J.-M. Tarascon and W. Van Schalkwijk, *Nat. Mater.*, 2005, **4**, 366-377.
8. A. Lamberti, N. Garino, A. Sacco, S. Bianco, D. Manfredi and C. Gerbaldi, *Electrochim. Acta*, 2013.
9. Z. Wang and X. W. D. Lou, *Adv. Mater.*, 2012, **24**, 4124-4129.
10. S. J. Ding, J. S. Chen, Z. Y. Wang, Y. L. Cheah, S. Madhavi, X. A. Hu and X. W. Lou, *J. Mater. Chem.*, 2011, **21**, 1677-1680.
11. J. S. Chen, Y. L. Tan, C. M. Li, Y. L. Cheah, D. Luan, S. Madhavi, F. Y. C. Boey, L. A. Archer and X. W. Lou, *J. Am. Chem. Soc.*, 2010, **132**, 6124-6130.
12. S. Liu, H. Jia, L. Han, J. Wang, P. Gao, D. Xu, J. Yang and S. Che, *Adv. Mater.*, 2012, **24**, 3201-3204.
13. M. Wagemaker and F. M. Mulder, *Acc. Chem. Res.*, 2012, **DOI: 10.1021/ar2001793**
14. Y. Ren, Z. Liu, F. Pourpoint, A. R. Armstrong, C. P. Grey and P. G. Bruce, *Angew. Chem.*, 2012, **124**, 2206-2209.
15. H. Li and H. Zhou, *Chem. Commun.*, 2012, **48**, 1201-1217.
16. C. Wang, H. Li, A. Fu, J. Liu, W. Ye, P. Guo, G. Pang and X. S. Zhao, *New J. Chem.*, 2014, **38**, 616-623.
17. K. Tang, L. J. Fu, R. J. White, L. H. Yu, M. M. Titirici, M. Antonietti and J. Maier, *Advanced Energy Materials*, 2012, **2**, 873-877.
18. Z. Q. Zhu, F. Y. Cheng, and J. Chen, *J. Mater. Chem. A*, 2013, **1**, 9484-9490.
19. L. Zhao, Y. S. Hu, H. Li, Z. Wang and L. Chen, *Adv. Mater.*, 2011, **23**, 1385-1388.
20. Z. Yang, G. Du, Q. Meng, Z. Guo, X. Yu, Z. Chen, T. Guo and R. Zeng, *J. Mater. Chem.*, 2012, **22**, 5848-5854.
21. S.-J. Park, H. Kim, Y.-J. Kim, H. Lee, *Electrochimica Acta*, 2011, **56**, 5355-5362.
22. S.-J. Park, Y.-J. Kim, H. Lee, *J. Power Sources*, 2011, **196**, 5133-5137.
23. W. Wang, Q. Sa, J. Chen, Y. Wang, H. Jung, Y. Yin, *ACS Applied Mater. Interfaces*, 2013, **5**, 6478-6483.
24. F.-F. Cao, X.-L. Wu, S. Xin, Y.-G. Guo and L.-J. Wan, *J. Phys. Chem. C*, 2010, **114**, 10308-10313.
25. N.D. Petkovich, S.G. Rudisill, B.E. Wilson, A. Mukherjee, A. Stein, *Inorg. Chem.*, 2014, **53**, 1100-1112.
26. B. Wang, H. Xin, X. Li, J. Cheng, G. Yang, F. Nie, *Sci. Rep.*, 2014, **4**: 3729, 1-7.
27. X. Jiang, T. Herricks and Y. Xia, *Adv. Mater.*, 2003, **15**, 1205-1209.
28. J. Zhang, X. H. Liu, S. R. Wang, S. H. Wu, B. Q. Cao and S. H. Zheng, *Powder Technol.*, 2012, **217**, 585-590.
29. K. Huang, Y. Li, Y. Xing, *J. Mater. Research*, 2013, **28**, 454-460.
30. L. Fu, H. Liu, H. Zhang, C. Li, T. Zhang, Y. Wu and H. Wu, *J. Power Sources*, 2006, **159**, 219-222.
31. Y. S. Hu, L. Kienle, Y. G. Guo and J. Maier, *Adv. Mater.*, 2006, **18**, 1421-1426.
32. J. Xu, C. Jia, B. Cao and W. Zhang, *Electrochim. Acta*, 2007, **52**, 8044-8047.
33. A. R. Armstrong, G. Armstrong, J. Canales, R. García and P. G. Bruce, *Adv. Mater.*, 2005, **17**, 862-865.
34. Z. Hong, M. Wei, T. Lan and G. Cao, *Nano Energy*, 2012, **1**, 466-471.
35. L. Zeng, C. Zheng, L. Xia, Y. Wang and M. Wei, *Journal of Materials Chemistry A*, 2013, **1**, 4293-4299.
36. V. G. Pol, S.-H. Kang, J. M. Calderon-Moreno, C. S. Johnson and M. M. Thackeray, *J. Power Sources*, 2010, **195**, 5039-5043.
37. A. K. Rai, L. T. Anh, J. Gim, V. Mathew, J. Kang, B. J. Paul, J. Song and J. Kim, *Electrochim. Acta*, 2013, **90**, 112-118.
38. Z. Yang, D. Choi, S. Kerisit, K. M. Rosso, D. Wang, J. Zhang, G. Graff and J. Liu, *J. Power Sources*, 2009, **192**, 588-598.
39. M. Reddy, G. Subba Rao and B. Chowdari, *Chem. Rev.*, 2013.
40. L. Liu, Q. Fan, C. Sun, X. Gu, H. Li, F. Gao, Y. Chen and L. Dong, *J. Power Sources*, 2012, **221**, 141-148.

1